Supporting Information for "Constraining microfractures in foliated Alpine Fault rocks with laser ultrasonics"

Jonathan Simpson[1,2], Ludmila Adam[3], Kasper van Wijk[1,2], and Jirapat Charoensawan[3]

[1]The Dodd-Walls Centre for Photonic and Quantum Technologies

[2]Physical Acoustics Laboratory, Department of Physics, University of Auckland, Auckland, New Zealand

[3]Physics of Rocks Laboratory, School of Environment, University of Auckland, Auckland, New Zealand

Contents of this file

Corresponding author: Jonathan Simpson, Physical Acoustics Laboratory, Department of Physics, University of Auckland, Auckland, New Zealand. (jsim921@aucklanduni.ac.nz)

Introduction

In this supporting information, we present thin section microphotographs of the samples used in the study, along with complete mineral compositions estimated from EBSD data (Section S1). We also present example wavefields of the ultramylonite sample, from which P-wave arrivals are picked (Section S2). Finally, we give a detailed overview of the methodology used for the differential effective medium (DEM) modeling, and present complete results for the average best-fitting models (Section S3).

Please note that all experimental data and software written for processing and analysis is available at the online repository, accessible via the DOI: `10.17608/k6.auckland.c.4841352` (Simpson et al., 2020). In the repository we include the raw experimental waveform data, P-wave arrival picks for all scans, short Python scripts to create the plots in this study, and the software for the DEM modeling, adapted after Kim, Kim, and Mainprice (2019). Additionally, the PlaceScan classes and functions used for processing and analysis are available at `https://github.com/jsimpsonUoA/PlaceScan`.

Text S1: Sample Mineral Compositions and Microphotographs

Figure S1 shows thin section microphotographs of the five rock samples. The planes of the thin sections are oriented perpendicular to the plane of visible foliation. Cross-polarized light is used to identify the minerals, in particular, micas. The schist, protomylonite, and mylonite display alternating millimeter to sub-millimeter bands of mica and quartz/feldspar. These micas are mostly aligned with the rock foliation, except for areas where the basal planes of the micas surround larger grains. The ultramylonite matrix has finer grains of interspersed mica and quartz/feldspar, with several larger parallel mica lenses. Minerals are difficult to identify in the cataclasite due to finer grains and because the thin section has a greater thickness due to the unconsolidated nature of the rock.

Table S1 gives the mineral compositions of the schist, protomylonite, mylonite, and ultramylonite samples as estimated from electron back-scatter diffraction (EBSD) images of the thin sections. These data (mineral phase distribution and crystal preferred orientation) are used to model the background anisotropic wave speed of our rocks using the MTEX code (Mainprice et al., 2015). Overall, the mineral compositions of these mylonitic and schist samples are very similar, meaning the background (microfracture free) wave speeds in these rocks are comparable.

Text S2: Wavefield data

Figure S2 shows the wavefields in the ultramylonite sample as a function of angular orientation for effective pressures of 2 MPa and 14 MPa. The black lines denote the P-wave arrival time which was picked in the waveforms at each angular orientation. As pressure increases, the average arrival time decreases, corresponding to an overall increase

in P-wave velocity. Moreover, the difference between the earliest and latest arrival times decreases between 2 MPa and 14 MPa, representing a decrease in the P-wave anisotropy.

Text S3: Details of the DEM Methodology and Results

The differential effective medium (DEM) modeling uses the modeling scheme of Kim et al. (2019), but we modify their GassDEM MATLAB code to add multiple sets of fractures. For each mylonitic and schist rock, we use the elastic stiffness matrices determined from MTEX modeling (Mainprice et al., 2015) of the EBSD data as our anisotropic background medium. The cataclasite is not modeled with the DEM approach as its porosity is too high for the assumptions of DEM and matrix wave speeds are unknown (no EBSD analysis was performed on that sample as it is too finely grained). Fractures are modeled as ellipsoids with X:Y:Z aspect ratios between 10:10:1 and 100:100:1. To model randomly oriented fractures, we impose 100 sets of air-filled ellipsoidal microfractures onto the background, each with unique randomly-selected 3D orientations. We also add a set of fractures whose plane is aligned with the plane of mineral foliation. By varying the relative volume percentages of randomly oriented versus aligned fractures ($V_{\|}$), we investigate how foliation-parallel microfractures affect the P-wave velocities.

One model consists of a single fracture shape and percentage of aligned versus randomly oriented fractures. We note that, in reality, elongated and rounded porosity probably coexist in these samples at high pressures. However, since we found that spherical pores have insignificant effects on wave speeds compared to elongated pores and to limit the number of free parameters, we do not include mixtures of pore shapes in our modeling. The GassDEM code calculates effective elastic stiffness matrices for total fracture vol-

umes (porosities) between 0% and 6% at 0.1% increments (measured porosities at room conditions were less than 6% for these rocks). We vary the fracture shape from 10:10:1 to 100:100:1 at increments of 10 and the percentage of fractures aligned with foliation from $V_{\parallel} = 5\%$ to $V_{\parallel} = 60\%$ at increments of 5%, computing the DEM model for every combination. We chose the upper limits of these parameters by determining which aspect ratio and $V_{\parallel}$ caused wave speeds consistently lower than our measured wave speeds. In total, 7320 elastic stiffness models are generated for each rock. For each model, we calculate the azimuthal P-wave group velocities using the relevant equations for transversely isotropic media (Simpson, 2019). Both the laser data and the EBSD mineral elastic stiffness matrices show that our assumption of transverse isotropy is a good approximation for these rocks.

The goodness-of-fit of each model is evaluated using the total sum of residuals between the model and experimental data at each angle. We also impose the constraint that fractures at higher pressures have a more rounded shape (lower aspect ratio), and that total porosity must decrease with pressure. For the schist, mylonite, and ultramylonite, the experimental data at 1 MPa and 16 MPa is compared with the models. Models are compared to the experimental data at 6 MPa rather than 1 MPa for the protomylonite, due to the anomalously low velocities at 1 MPa thought to be caused by a macroscopic fracture. To prevent over-fitting the data, we select the 10 best-fitting DEM models at each pressure to calculate average values for fracture volume, percentage of aligned fractures, and fracture shape. These results are reported in Table S2.

References

Kim, E., Kim, Y. H., & Mainprice, D. (2019). GassDem: A MATLAB program for modeling the anisotropic seismic properties of porous medium using differential effective medium theory and Gassmann's poroelastic relationship. *Computers and Geosciences*, *126*, 131–141. doi: 10.1016/j.cageo.2019.02.008

Mainprice, D., Bachmann, F., Hielscher, R., Schaeben, H., & Lloyd, G. E. (2015). Calculating anisotropic piezoelectric properties from texture data using the MTEX open source package. *Geological Society, London, Special Publications*, *409*(1), 223–249.

Simpson, J. (2019). *Non-contact measurements to estimate the elastic properties of rocks under in situ conditions* (Masters Thesis). The University of Auckland.

Simpson, J., Adam, L., van Wijk, K., & Charoensawan, J. (2020). *Data and software for manuscript "Constraining microfractures in foliated Alpine Fault rocks with laser ultrasonics".* figshare. Retrieved from `https://auckland.figshare.com/collections/Data_and_software_for_manuscript_Constraining_microfractures_in_foliated_Alpine_Fault_rocks_with_laser_ultrasonics_/4841352/1` doi: 10.17608/k6.auckland.c.4841352

Table S1. Mineral volume percentages determined from EBSD-SEM images for four of the five Alpine Fault samples.

	Mica (%)	Quartz (%)	Feldspar (%)
Schist	22	42	36
Protomylonite	20	56	24
Mylonite	32	31	37
Ultramylonite	29	31	40

Table S2. Average values and standard deviations of the ten best-fitting DEM models for each sample. Aspect ratios indicate the (equal) X and Y dimensions of the ellipsoidal X:Y:1-shaped fractures. The low pressure is $P_{\text{Low}} = 6$ MPa for the protomylonite, and $P_{\text{Low}} = 1$ MPa for the other samples. $P_{\text{High}} = 16$ MPa for all samples.

	Percentage of Fractures $\parallel$ to Foliation, $V_{\parallel}$	Aspect Ratio at P_{Low}	Aspect Ratio at P_{High}	Porosity at P_{Low} (%)	Porosity at P_{High} (%)
Schist	30 ± 3	65 ± 10	43 ± 11	1.9 ± 0.2	1.1 ± 0.3
Protomylonite	25 ± 3	67 ± 15	52 ± 16	1.3 ± 0.5	0.9 ± 0.3
Mylonite	16 ± 4	59 ± 13	43 ± 11	1.7 ± 0.5	1.3 ± 0.3
Ultramylonite	40 ± 2	88 ± 23	72 ± 22	3.3 ± 1.1	2.7 ± 1.0

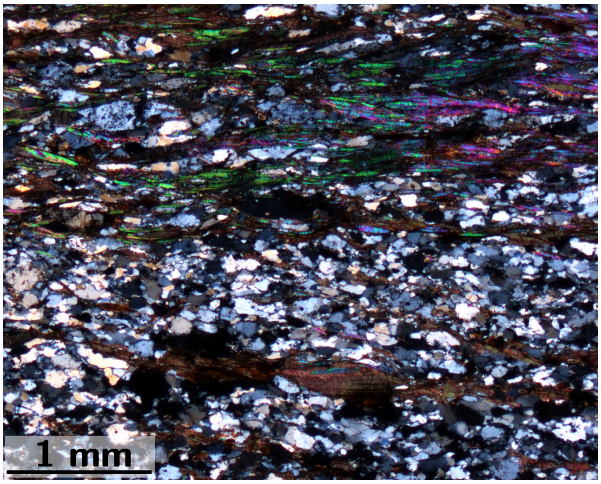

Schist

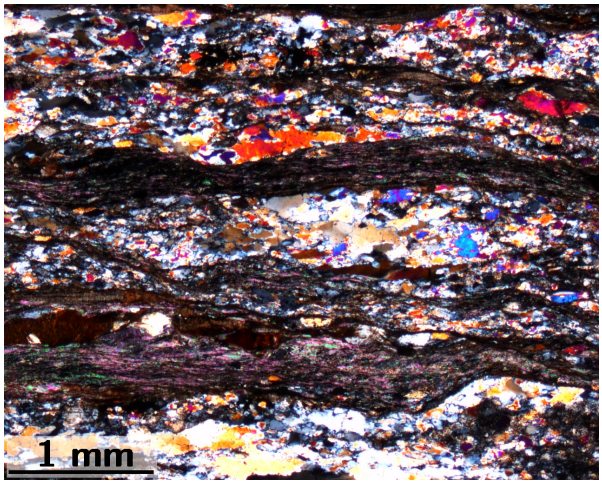

Protomylonite

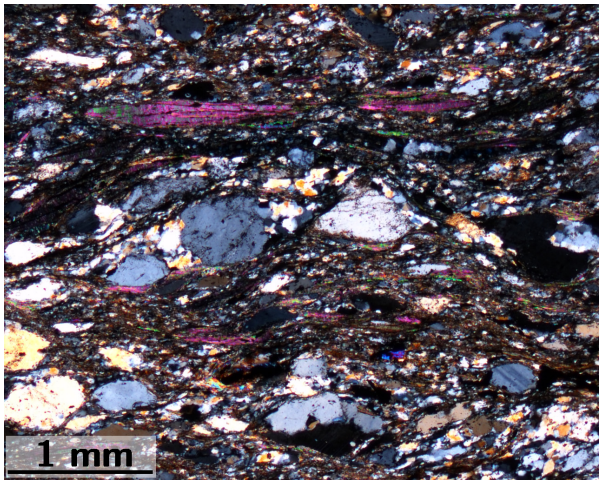

Mylonite

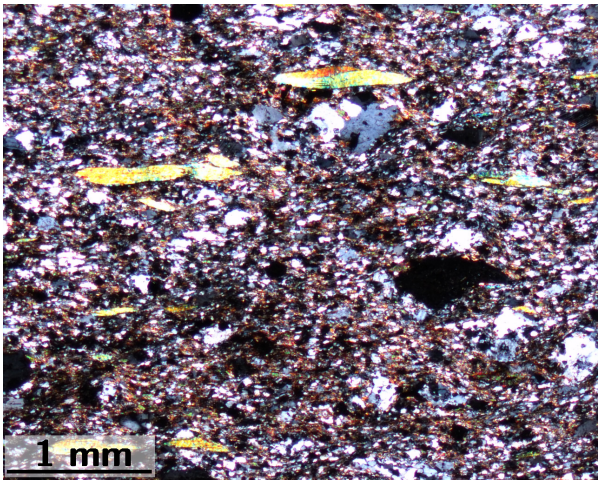

Ultramylonite

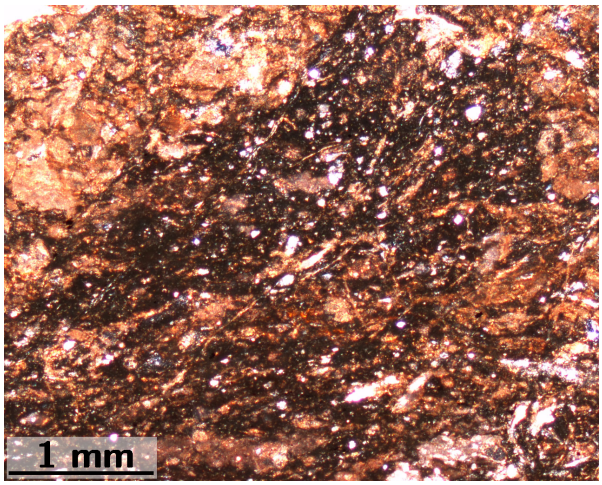

Cataclasite

February 4, 2020, 3:05pm

Figure S1. Microphotographs (cross-polarized light) of the Alpine Fault rock samples.

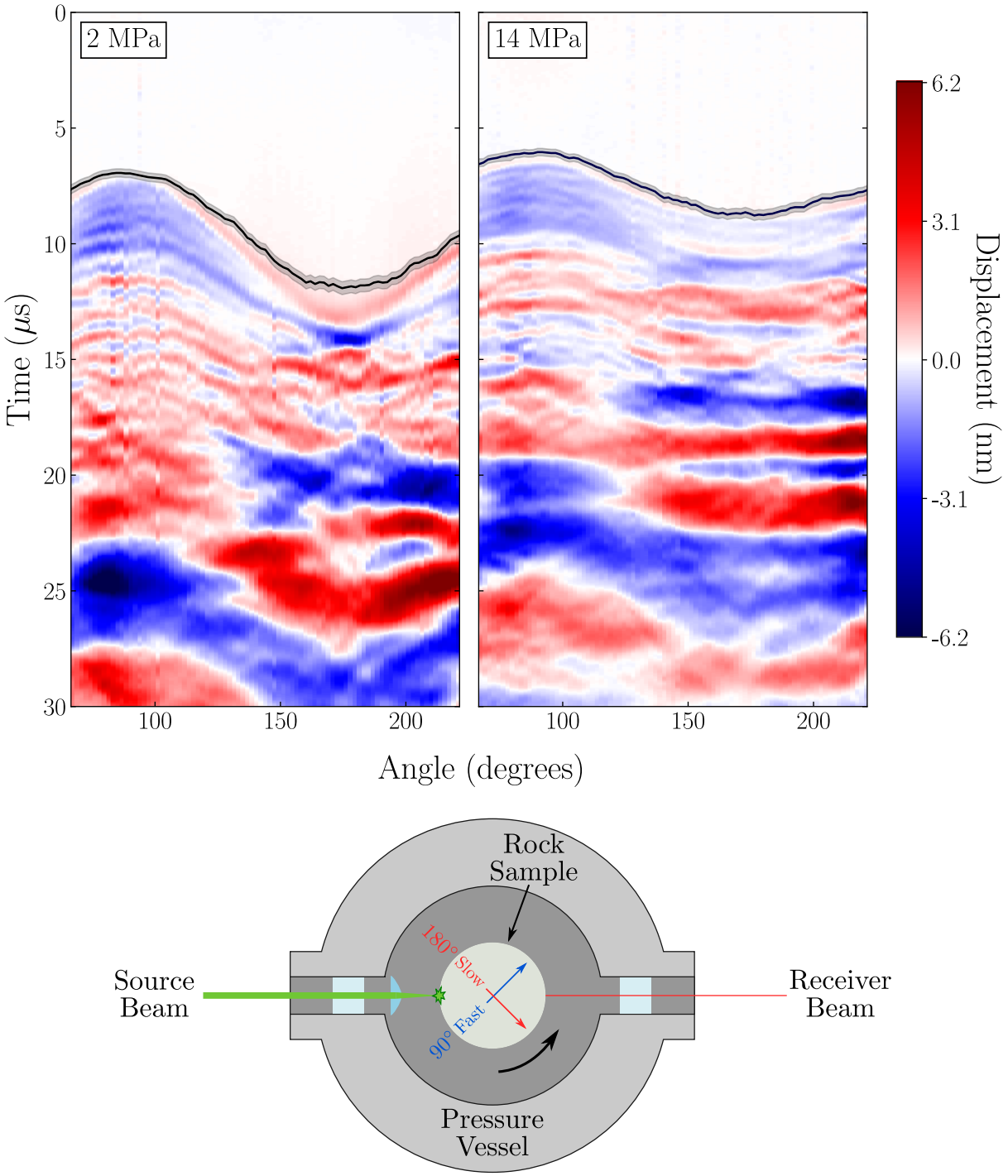

Figure S2. Wavefields as a function of angle recorded at 2 MPa and 14 MPa for the ultramylonite sample. The color scale show the absolute displacement of the sample surface as recorded by the laser Doppler vibrometer. Black lines denote the P-wave arrival time picks. The schematic below the wavefields shows a top-down view of the experimental configuration, denoting the relative orientations of the fast and slow directions in the wavefield plots.